

An 8-bit In Resistive Memory Computing Core with Regulated Passive Neuron and Bit Line Weight Mapping

Yewei Zhang, *Student Member, IEEE*, Kejie Huang, *Senior Member, IEEE*, Rui Xiao, *Student Member, IEEE*, and Haibin Shen

Abstract—The rapid development of Artificial Intelligence (AI) and Internet of Things (IoT) increases the requirement for edge computing with low power and relatively high processing speed devices. The Computing-In-Memory (CIM) schemes based on emerging resistive Non-Volatile Memory (NVM) show great potential in reducing the power consumption for AI computing. However, the device inconsistency of the non-volatile memory may significantly degenerate the performance of the neural network. In this paper, we propose a low power Resistive RAM (RRAM) based CIM core to not only achieve high computing efficiency but also greatly enhance the robustness by bit line regulator and bit line weight mapping algorithm. The simulation results show that the power consumption of our proposed 8-bit CIM core is only 3.61mW (256*256). The SFDR and SNDR of the CIM core achieve 59.13 dB and 46.13 dB, respectively. The proposed bit line weight mapping scheme improves the top-1 accuracy by 2.46% and 3.47% for AlexNet and VGG16 on ImageNet Large Scale Visual Recognition Competition 2012 (ILSVRC 2012) in 8-bit mode, respectively.

Index Terms—In-memory computing, Non-volatile memory, Neuromorphic chip, Resistance inconsistency, Weight quantization and mapping

I. INTRODUCTION

IN the past decade, with internet of things, cloud computing, computer vision, and artificial intelligence becoming increasingly connected to do perception, cognition, decision, and interaction, sensing devices in intelligent products are going to be the key interfaces to the real world. However, communication, storage, information retrieval, computation, and recognition will face great challenges due to the extremely large amount of sensing data. Because of the separation of the data acquisition, processing, and analysis, the conventional intelligent systems are suffering from problems like high construction cost, high power consumption, low efficiency, and long latency [1]. To address these issues, the majority of AI computations will be moved to light-weight IoT devices [2]. Nevertheless, Moores Law has come to the end and the processor performance will be benefited little from Complementary Metal Oxide Semiconductor (CMOS) technology node scaling down. Therefore, we have to design new hardware architectures and software algorithms to meet

the requirement of the perception, computation, and storage at the end devices with limited computation capability and storage resources.

The high density and low power emerging resistive Non-Volatile Memory (NVM) [3]–[11] which enables massive parallel Computing In-Memory (CIM) is a promising candidate to solve the above-mentioned issues [12]–[14]. The majority of works are utilizing the multilevel resistance of the resistive memory for both storage and computation [15]–[18]. For example, Hewlett Packard Laboratories (HPL) proposed a Dot Product Engine (DPE) with the inverting amplifier [19]. [20] designed In-Situ Analog Arithmetic in Crossbars (ISAAC) which utilizes eight 4 level RRAM cells to represent 16-bit weight. Though resistive NVM provides a potential solution as the CIM unit, its non-ideal properties greatly degenerate the reliability of the system. A few widely known properties of resistive NVM are the non-linear resistance value with different biasing voltage, level to level resistance variation, and cell to cell resistance variation, which will cause significant errors in quantization, resulting in the accuracy loss in the network. To reduce the mapping errors and improve the linearity of the CIM system, a more reliable design is needed which may be at the cost of the increasing of the computing energy.

[21], [22] proposed Serial-Input Non-Weighted Product (SINWP) whose inputs are modulated by time instead of the analog voltage, which will address the non-linearity issue caused by the biasing voltage. However, the digital-to-time converter will greatly increase the computing time at high data width. [23] proposed a novel Multiple Binary RRAM with Active Integrator (MBRAI) CIM core architecture, where multiple binary RRAM cells are used to store one weight. MBRAI could save a lot of power because binary code is used at the input instead of a time signal. Therefore, it requires only n CIM computations instead of 2^n . The n -bit input data are sequentially computed by the CIM core and weighted at the output neurons, which greatly improves the linearity because of the identical input voltage. However, the power consumption of this scheme is dominated by the operational amplifier (>95%) [23], which reduces the computing efficiency of the CIM core to 0.61 Tera-Multiply-Accumulates per Second per Watt (TMACs/s/W). What's more, the accuracy is still be influenced by the quantization and the inconstancy of the resistive NVM cells. To reduce power consumption, a CIM core with regulated passive integrators is proposed in this paper. A pseudo-binary weight quantization and bit line weight mapping method aimed at solving the resistance inconsistency is also introduced. The simulation results show that the power

Authors: K. Huang and H. Shen are with the College of Information Science & Electronic Engineering, Zhejiang University, 38 Zheda Road, Hangzhou, China, 310027, and also with Zhejiang Lab, Building 10, China Artificial Intelligence Town, 1818 Wenyi West Road, Hangzhou City, Zhejiang Province, China, email: huangkejie@zju.edu.cn; shen_hb@zju.edu.cn Y. Zhang and R. Xiao are with the College of Information Science & Electronic Engineering, Zhejiang University, 38 Zheda Road, Hangzhou, China, 310027, email: yeweizhang@zju.edu.cn; xiaor@zju.edu.cn

consumption of the proposed 256*256 CIM core in 8-bit mode is reduced by 98.2% compared with MBRAI.

The rest of this paper is organized in the following manner. Section II introduces the background of CIM with resistive NVMs. Section III shows the proposed circuit, problems brought by resistance inconsistency, and corresponding optimization. Finally, simulation results are presented in Section IV with the conclusion in Section V.

II. BACKGROUND AND RELATED WORKS

The majority of the computations in the neural network are matrix multiplication and accumulate operations, which can be well implemented by crossbar architecture as shown in Fig. 1. The processing units shown as black dots multiply the input from word lines by the stored weight. The neuron represented by the triangle accumulates the multiplication results at the same bit line.

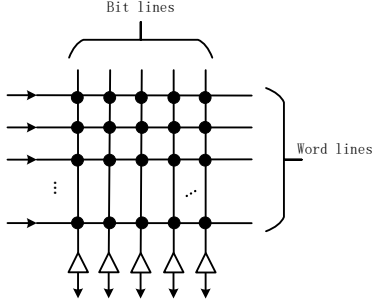


Fig. 1. Microarchitecture of a CIM core. The word lines get input data from the former neurons while the bit lines is to accumulate data at the neurons (triangles). The black dots are the computing unit.

In conventional schemes, the weight of the neural network is stored in SRAM. For example, [24] proposed a 7-bit input and 1-bit weight MAC using a 10T SRAM cell. However, the precision is limited by the 1-bit weight and the area is large due to the SRAM array. Emerging NVMs which have high density and simpler structure as memory unit will greatly improve the precision of the weight and reduce the

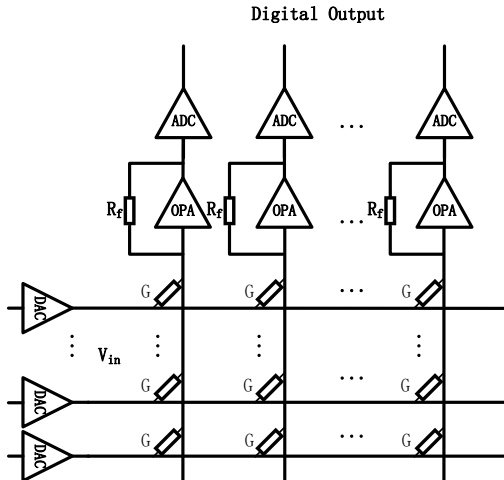


Fig. 2. Basic architecture of HPL's Dot-Product Engine

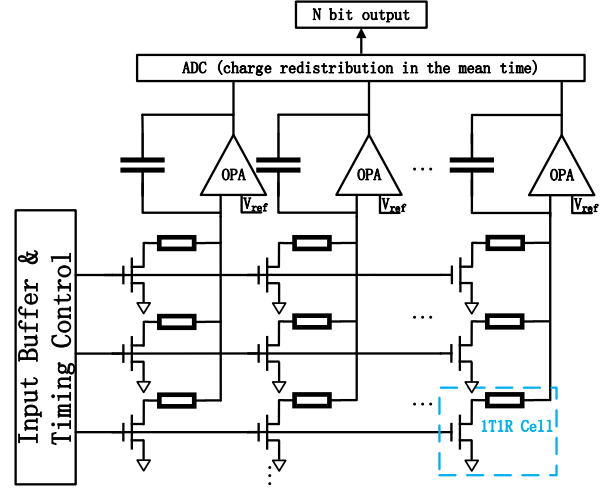


Fig. 3. Simplified integration circuit with OPA.

core area for its application on CIM. A design of CIM core with NVM in DPE is shown in Fig. 2. It employs memristor crossbar for matrix multiplication where memristor stores the weight by its resistance. Once the input is converted to analog voltage by DAC, the output voltage is determined by the conductance of the resistance as $V_{out} = \sum V_{in} G R_f$, where R_f is the feedback resistance, and G is the conductance of the cross-point memristor device. After that, the output voltage is digitalized by the ADC for data transmission. DAC and ADC, which are power-hungry components, are necessary to resist the noise and signal deformation in data transmission. MBRAI proposed in [23] moves the input DACs to the output and shares the ADC for lower power consumption. RRAM is chosen as the storage unit for its reconfigurability, high density, and low power consumption. However, it is a great challenge to precisely control the resistance value of RRAM. Therefore, MBRAI utilizes n RRAM cells with binary resistance states whose high resistance state (HRS) is 0 and low resistance state (LRS) is 1, to represent an n -bits weight to achieve a high Effective Number of Bits (ENOB) for weight mapping. Fig. 3 is the simplified integration circuit of MBRAI. The input is sent in bit by bit from Least Significant Bit (LSB) to Most Significant Bit (MSB), which is more computing reliable since every bit is identical in computation. The importance of each bit of the input data and network weights are weighted by the charge redistribution at the neurons.

Though MBRAI achieves better computing reliability, there are still two critical issues that need to be addressed. Firstly, the power consumed by amplifiers in active integrators accounts for more than 95% of the energy cost of the whole CIM core. Secondly, the resistance of the RRAM cells has a wide distribution, resulting in significant quantization errors when mapping weights of the neural network into the RRAM array. To address the first issue, a passive integrator is proposed. A regulator is designed to improve the linearity of the integration results. The details will be introduced in Section III.A. To address the second issue, a pseudo-binary quantization and bit line weight mapping method is proposed to reduce the impact

of the resistance inconsistency. The details will be introduced in Section III.B.

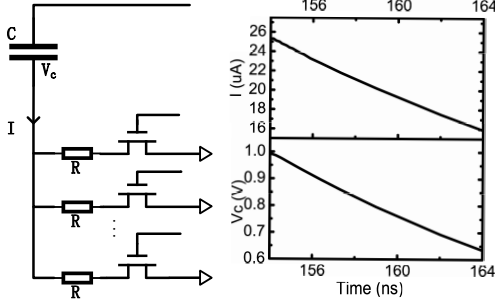


Fig. 4. Passive integrator with amplifier removed and its integration process.

III. PROPOSED CIM CORE AND MAPPING METHOD

Although a passive integrator can significantly reduce power consumption by removing the amplifier, it has a serious non-linear problem. Fig. 4 shows the passive integrator circuit and its integration process where the current decreases with the decreasing of the integrating voltage V_C . To improve the linearity of the circuit, we design an optimized n-bit integral multiplier shown in Fig. 5:

- 1) We switch the position of RRAM and transistor in 1T1R so that the reading voltage on the RRAM cell is mainly determined by the gate and threshold voltages of the transistor. To differentiate from the conventional structure, the new structure is named as 1R1T.
- 2) The saturation current of the transistor in 1R1T can be influenced by the change of the integrating voltage because of the channel length modulation effect. To minimize the impact of the integrating voltage, we add NMOS T_0 at bit line to isolate the integrating voltage and drain voltage of 1R1T and thus reduce the variation of the integrating current.
- 3) Because the load of the bit line is affected by the number of input lines and the weights' values, the linearity of the circuit is still influenced by the change of the source voltage of T_0 (the drain voltage of the 1R1T). Therefore, a regulator is added at T_0 to make sure the stability of the drain voltage of 1R1T.
- 4) Besides the nonlinearity in the bit line voltage, the cell to cell variation makes the devices' integrating current inconsistent which decreases the robustness of the system. To improve reliability, we propose a pseudo-binary quantization and bit line weight mapping method with corresponding circuit which utilizes the uncertainty of resistive NVM to reduce quantization error.

A. CIM Core with Regulated Passive Integrator

1) *Core Design:* Assuming the n-bit input sequence is X_1, X_2, \dots, X_l and the weight is W_1, W_2, \dots, W_l , the

multiplication and accumulation(MAC) can be expressed as

$$Y = \sum_{i=1}^l X_i W_i = \sum_{i=1}^l \sum_{j=0}^{n-1} 2^j x_{i,j} w_{i,j} \quad (1)$$

$$= \sum_{i=1}^l \sum_{j=0}^{n-1} 2^j \sum_{k=0}^{n-1} 2^k x_{i,j} w_{i,k}$$

where $x_{i,n-1}x_{i,n-2}\dots x_{i,0}$ and $w_{i,n-1}w_{i,n-2}\dots w_{i,0}$ is the binary format of X_i and W_i ($x_{i,j}, w_{i,k} \in (0, 1)$), respectively. It can be observed from Eq. 1 that there are three consecutive accumulations. The proposed CIM core utilizes n integrator cells to get $\sum_{i=1}^l x_{i,j} w_{i,k}$ by charge integration, and the results are stored in the passive regulated neuron composed by the capacitance array in Fig. 5 for charge redistribution to get the $\sum_{i=1}^l x_{i,j} W_i$. The $\sum_{i=1}^l x_{i,j} W_i$ is also added up by charge redistribution to get $\sum_{i=1}^l X_i W_i$. The integration for the resistances in the same bit line will be finished simultaneously by sharing the integrator so that the MAC can be finished parallelly to achieve a smaller core area and faster computing speed. Multiple neurons are enabled at a time in the integration phase when the inputs are divided into n cycles and calculated from LSB to MSB. After integration and charge redistribution, the data conversion phase is started for neurons to convert the analog results into digital output.

2) *Integral Multiplier:* The word line inputs shown in Fig. 5 are sent in once a bit from LSB to MSB. The process of multiplication in the integral multiplier includes the integration phase and the charge redistribution phase. When in the integration phase, S_2 is closed, S_1, S_3 , and S_4 are open. After the integration, the charge is redistributed with S_1 and S_2 open and S_3 and S_4 closed in the charge redistribution phase. Taking C_{n-1} as an example, the integrating voltage after the integration phase is

$$V_{c,n-1} = V_{c,n-1}^- - \frac{V_{D2} \sum_{i=0}^{l-1} D_i T}{C_f R_i} \quad (2)$$

where $V_{c,n-1}^-$ is the initial voltage of C_{n-1} , D_i is one input bit of the i_{th} input line, l is the number of input lines, T is the integration time, R_i is the equivalent resistance of the 1R1T unit of the i_{th} input line and V_{D2} is the drain voltage of 1R1T unit. The capacitances satisfy the following constraint

$$C_f = 2C_{n-1} = 2^2 C_{n-2} = 2^3 C_{n-3} = \dots = 2^n C_0 \quad (3)$$

Assuming there is only one input line and the initial integrating voltage is set to V_C^- , the integrating voltage V_S after one step of charge redistribution is

$$V_S = \frac{V_{c,n-1} C_{n-1} + V_{c,n-2} C_{n-2} + \dots + V_{c,0} C_0 + V_C^- C_0}{C_{n-1} + C_{n-2} + \dots + 2C_0}$$

$$= V_C^- - \frac{V_{D2} T}{C_f} \left(2^{-1} \sum_{i=0}^{l-1} \frac{D_{i,n-1}}{R_{i,n-1}} + 2^{-2} \sum_{i=0}^{l-1} \frac{D_{i,n-2}}{R_{i,n-2}} \right.$$

$$\left. + \dots + 2^{-n} \sum_{i=0}^{l-1} \frac{D_{i,0}}{R_{i,0}} \right) \quad (4)$$

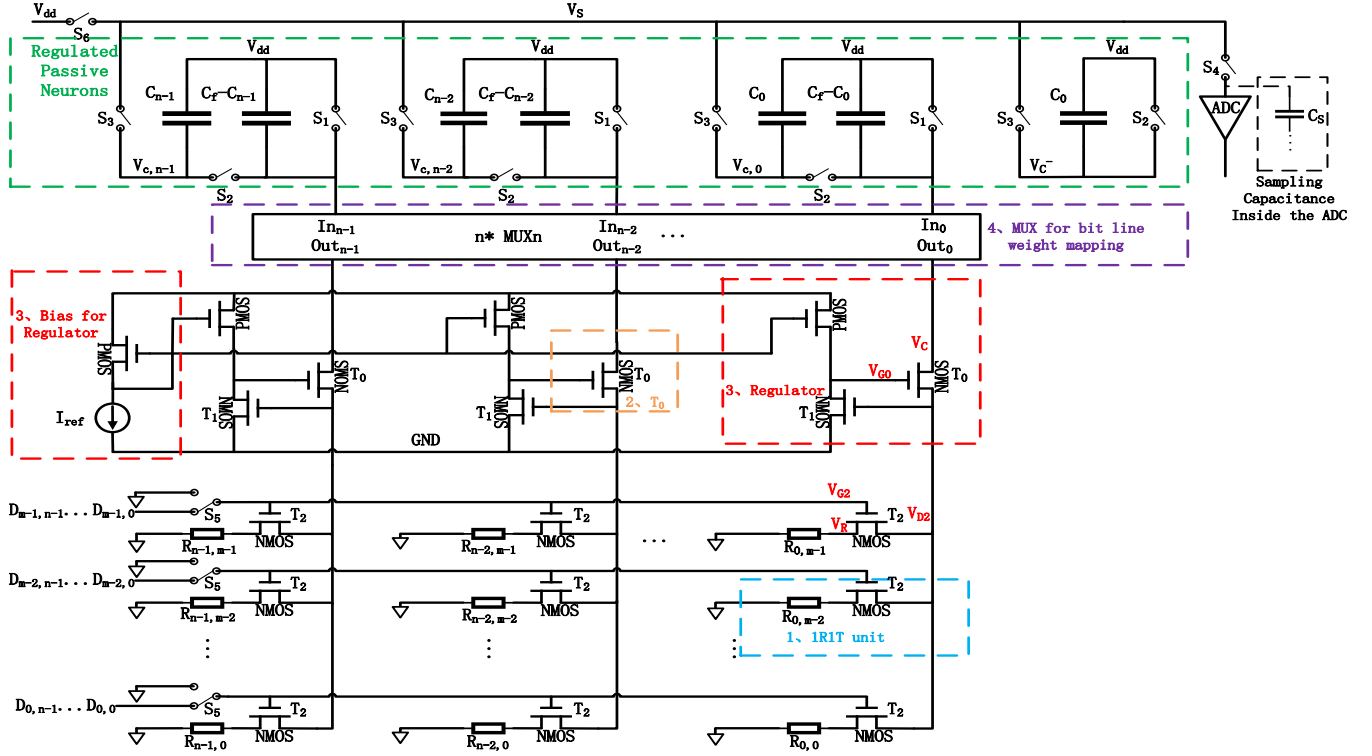


Fig. 5. Integration circuit without amplifier

ADC's sampling capacitance C_S which is connected to the integrator's capacitance array is in the meantime used to add up the n partial products. Let $C_S = C_f$, the new V_{out} is

$$V_{out} = 2^{-1} (V_S + V_{out}^-) \quad (5)$$

where V_{out}^- represents the former voltage of the C_S . Assuming the initial voltage of the C_S is V_{init} , then after n steps of the charge redistribution, the voltage change is

$$\begin{aligned} \Delta V_{out} &= V_{init} - (2^{-n} V_{init} + 2^{-n} V_{S,0} + \dots + 2^{-1} V_{S,n-1}) \\ &= 2^{-n} [(V_{init} - V_{S,0}) + \dots + 2^{n-1} (V_{init} - V_{S,n-1})] \\ &= 2^{-n} \sum_{j=0}^{n-1} 2^j \Delta V_{S,j} \end{aligned} \quad (6)$$

where $V_{S,n-1}$ is the $(n-1)_{th}$ integrating voltage of V_S and $\Delta V_{S,j}$ is the voltage change of V_S in the j_{th} integration. As long as the $\Delta V_{S,j}$ is designed to represent the result of the $\sum_{i=0}^l x_{i,j} W_i$, Eq. 6 gives the result of $\sum_{i=0}^l \sum_{j=0}^7 2^j x_{i,j} W_i$.

3) *Regulated Passive Integrator*: By switching the position of 1T1R in Fig. 3 to 1R1T in Fig. 5, we can get the following equations

$$I = \frac{1}{2} K_2 (V_{G2} - V_R - V_{th2})^2 \quad (7)$$

$$I = \frac{V_R}{R} \quad (8)$$

where K_2 is the device parameter of T_2 , V_{th2} is its threshold voltage, R is the resistance of RRAM device, V_R is resistance's

read voltage, I is the integrating current passing through the 1R1T unit. According to Eq. 7 8, we can get

$$V_R = V_{G2} - V_{th2} - \frac{\sqrt{2K_2 R (V_{G2} - V_{th2}) + 1} - 1}{K_2 R} \quad (9)$$

The drain voltage of T_2 (V_{D2}), which is isolated from the integrating voltage by T_0 , satisfies the following equation

$$I_b = \frac{1}{2} K_0 (V_{G0} - V_{D2} - V_{th0})^2 \quad (10)$$

where I_b is the integrating current of the bit line, K_0 is the device parameter of T_0 . The proposed regulator circuit shown in Fig. 5 stabilizes the V_{D2} of the 1R1T units by applying a negative feedback. T_1 works at the saturation region, which satisfies the following equation

$$I_{ref} = \frac{1}{2} K_1 (V_{D2} - V_{th1})^2 \quad (11)$$

where K_1 is the device parameter of T_1 , V_{th1} is the threshold voltage of T_1 . According to Eq. 10 11, we get

$$V_{G0} = V_{th1} + \sqrt{\frac{I_{ref}}{K_1}} + V_{th0} + \sqrt{\frac{I_b}{K_0}} \quad (12)$$

$$V_{D2} = V_{th1} + \sqrt{\frac{I_{ref}}{K_1}} \quad (13)$$

Since I_{ref} is a constant, the drain voltage V_{D2} of the 1R1T unit is stabilized by the regulator.

B. Pseudo-binary Quantization and Bit Line Weight Mapping Method

As the weight of the neural network is quantized to n bits rather than a continuous value, the quantization errors when mapping the weight of the neural network into the CIM system will influence the accuracy of inference. What's more, the resistance distribution of resistive NVM may worsen the quantization. Therefore, it's necessary to discuss the quantization method and the corresponding errors in this section. To reduce the quantization error caused by the cell to cell variation, a pseudo-binary quantization and bit line weight mapping method is proposed.

1) *Quantization Error with NVM*: Quantization is an important method for compressing the neural network and accelerating the computation speed, among which uniform quantization is a basic one. The typical quantizer of uniform quantization can be expressed as

$$Q(x) = \Delta \cdot \left\lfloor \frac{x}{\Delta} + \frac{1}{2} \right\rfloor \quad (14)$$

where Δ is the quantization step size of some value, x is the value to be quantized. When the quantization step size (Δ) is small relative to the variation in the signal being quantized, it is simple to show that the mean squared error which is also called the quantization noise power produced by such a rounding operation will be $\frac{\Delta^2}{12}$. The calculation process is

$$QE = \int_0^{\frac{\Delta}{2}} \frac{x^2}{\frac{\Delta}{2}} dx = \frac{\Delta^2}{12} \quad (15)$$

The maximum (w_{max}) and the minimize (w_{min}) of the data range and the quantization bits n determine the quantization step size since they usually have the relationship

$$\Delta \times 2^n = (w_{max} - w_{min}) \quad (16)$$

Considering the resistance distribution, the practical non-linear quantizer is shown as follows

$$\sum_{i=1}^{2^n} \Delta_i = (w_{max} - w_{min}) \quad (17)$$

Assuming the resistance distribution is a general normal distribution represented as

$$f(x|\mu, \sigma^2) = \frac{1}{\sqrt{2\pi\sigma^2}} e^{-\frac{(x-\mu)^2}{2\sigma^2}} \quad (18)$$

The Probability Density Function (PDF) of the quantization error is the noncentral chi-squared distribution with one degree of freedom. Then, the mean value of the quantization error is given by

$$\mu = k + \frac{\lambda}{12} = 1 + \frac{\mu^2}{12} = 1 + \frac{\Delta^2}{12} = 1 + \frac{(w_{max} - w_{min})^2}{12 \times 2^{2n}} \quad (19)$$

and the variance of the quantization error is

$$\begin{aligned} \sigma^2 &= 2(k + 2\lambda) = 2 + 4\mu^2 = 2 + 4\Delta^2 \\ &= 2 + \frac{(w_{max} - w_{min})^2}{2^{2(n-1)}} \end{aligned} \quad (20)$$

As we can see, the quantization error is greatly increased when there is a distribution in resistance. Since the quantization errors are accumulated in the network, the accuracy will be greatly reduced.

2) *Resistance Measurement*: The proposed quantization and mapping method needs the resistance value of the RRAM array in LRS, so we firstly set all memory units to LRS and read the resistance of the RRAM array by ADC in resistance reading phase. The reading process consists of integration phase and charge redistribution phase when the switches are set different from multiplication. For example, when reading the resistance unit $R_{n-1,m-1}$ in Fig. 5, the switches in the same bit line with $R_{n-1,m-1}$ are used while the others stay open. In the integration phase, S_1 , S_3 , and S_4 are open, S_2 is closed and the input of $(m-1)_{th}$ word line is 1 while the others are 0. The integration result is a typical result of Eq. 2 where $l=1$, $D=1$. When ADC read the integrating voltage during the charge redistribution, S_2 , S_3 , and S_4 are closed and S_1 is open. The voltage read by ADC is

$$V_{out} = \frac{V_{init} + V_S}{2} \quad (21)$$

where V_{init} is the initial voltage for both sampling capacitances and integration capacitances, and V_S is the integration result. The integration process satisfies

$$V_{init} - V_S = \frac{IT}{C_f} = \frac{V_{D2}T}{RC_f} \quad (22)$$

where I is the integrating current passing through 1R1T unit, T is the integration time, R is 1R1T's resistance and V_{D2} is the read voltage of the bit line. Therefore, we can get

$$R = \frac{V_{RT}}{2C_f(V_{init} - V_{out})} \quad (23)$$

3) *Quantization and Mapping Method*: Since the normalized resistance in LRS is not exactly digital 1, a pseudo-binary code whose importance of bits from MSB to LSB is still the same as the conventional binary code is proposed in our mapping schemes. The main difference is that the value of the pseudo-binary code is related to the resistance of the memory unit, which is given by

$$\hat{w} = r_{n-1} \times 2^{n-1} + r_{n-2} \times 2^{n-2} + \dots + r_0 \times 2^0 \quad (24)$$

where for the LRS, r_i is the normalized resistance of the i_{th} bit (mean value is 1) of the weight. For the high resistance, since the resistance can be much larger than the low resistance, r_i is set as 0, and the uncertainty of the high resistance is ignored in this paper. The weight quantization procedure is from MSB to LSB and we define the condition as follows

$$q = ! \left[(r_i \times 2^{i-1} - w_{res} > 0.5) \mid (r_i \leq 0.5) \mid (r_i \times 2^{i-1} > 2 \times w_{res}) \right] \quad (25)$$

where r_i is the i_{th} bit of normalized memory resistance, and w_{res} is the remaining weight after partial quantization. The component $(r_i \leq 0.5)$ is to abandon the device with too large resistance in LRS and $r_i \times m_i - w_{res} > 0.5$ is to check if the remaining weight is larger than the product of

the importance of the bit and the resistance of the memory. The component $r_i \times m > 2 \times w_{res}$ is to minimize the quantization error of the LSB. Because of the memory resistance distribution, $|r_0 \times m_0 - w_{res}|$ could be larger than w_{res} . In other words, the memory should be in high resistance in case $|r_0 - w_{res}| > w_{res}$ to minimize the quantization errors.

However, the initial memory sequence may not be the best solution to minimize the quantization error. For example, assuming $w=13.4$, and four memory units with normalized resistance 1.05, 1.1, 1.125, 0.93 are used to quantize the weight. The conventional binary code may give a quantization error of 0.4 (4'b1101). Based on the given sequence, the resistance states of the four cells are low, low, high, low, which reduce the quantization error to -0.33. Furthermore, if we switch the third cell with MSB, the resistance of the four cells will be 1.125, 1.1, 1.05, and 0.93. In such a sequence, the resistance states of the four cells can be set to low, low, high, and high to minimize the quantization error to 0. This example shows that the sequence of the memory units is very important to minimize the quantization error.

The traversal algorithm can be used to search all possible sequences, and the sequence for the minimal quantization error is picked and configured in the chip. However, it may require a long searching time and its computation complexity is $O(n!)$. Moreover, the cells in the same bit line should be in the same sequential position. Assuming the size of the weight matrix need to be quantized is $R \times 1$ and the size of RRAM array is $R \times C$ where C means the weight is quantized to C bits, we propose a greedy mapping algorithm whose loss when quantizing the i_{th} bit is defined as

$$\text{loss} = \max_{j \in R} (w_{i-1,j} - \hat{w}_{i,j}) \sum_{j=1}^{j=R} (w_{i-1,j} - \hat{w}_{i,j})^2 \quad (26)$$

where $w_{i-1,j}$ is the remaining value of the j_{th} weight after partial quantization and $\hat{w}_{i,j}$ is the value quantized by the pseudo-binary quantization method in the i_{th} bit of the j_{th} row. Eq. 26 has taken both the worst case and the average case of the searching results into consideration. This bit line selection is started from MSB which influences the mapping result most to LSB. The algorithm traverses the remaining bit lines and chooses the bit line with minimum loss as the i_{th} bit. To apply the algorithm in the circuit, the $n \times \text{MUX}n$ in Fig. 5 is used for switching the connection between the bit lines of the RRAM array and the integrators. When mapping the weights to the core, all the RRAMs are set to LRS at first. Then, according to the proposed mapping method, RRAMs with value 0 are set to HRS. By using this bit line weight mapping method, the computation complexity is reduced from $O(n!)$ to $O(n^2)$.

IV. SIMULATION RESULTS

In this section, we do the functional verification of the multiplication and resistance reading process. Then we evaluate the circuit with dynamic performance, energy cost on circuit level and compare it with other CIM schemes on core level and network level. Finally, we present the robustness of the circuit. The circuit simulations are done in Cadence Analog

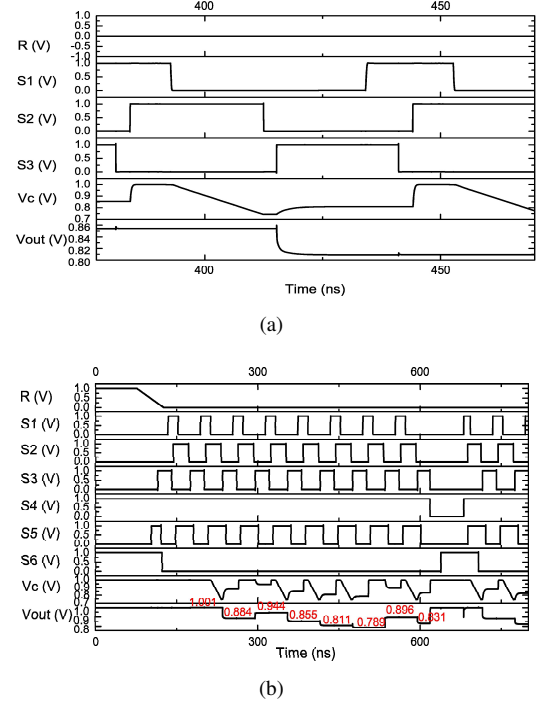


Fig. 6. Transient simulation results of (a) integration phase and charge redistribution phase for one bit of input (b) the core's multiplication process of 8'b10111010 as input and 8'b11101100 as weight.

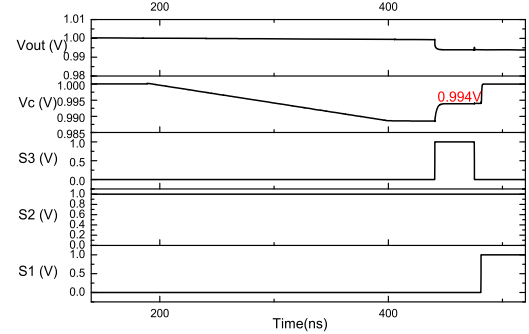


Fig. 7. Process of resistance reading where the state of the switches controlling it is presented

Mixed Signal (AMS) with a 45nm generic Process Design Kit (PDK) and the network simulations are done on caffe platform.

A. Functional Verification

1) *Multiplication Process Verification:* We simulate the computing process shown in Fig. 6 to check the correctness of the proposed circuit in 8-bit mode. Fig. 6(a) presents the integration phase in an integrator, the integrating voltage V_C shown in Fig. 5 is reset to 1V at 384 ns, and the integration phase starts at 393 ns. After 20 ns, the integration phase is completed and V_C is decreased to 745.2mV. Then the charge redistribution starts at 415 ns. When charge redistribution is done, the 8 integrating voltages are converted to V_{out} . After that, V_C is reset to 1V for the next integration. Fig. 6(b) shows the whole multiplication process of an 8-bit input (8'b10111010) and 8-bit weight (8'b11101100). The input

TABLE I
CIM CORE PERFORMANCE COMPARISON BETWEEN MBRAI AND THE PROPOSED

	MBRAI [23]	Proposed
Supply Voltage	1.1V	1V
Computing Speed	1.85M/s	1.85M/s
SFDR	67.42dB	59.13dB
SNDR	45.48dB	46.13dB
ENOB	7.26bit	7.37bit

TABLE II
ENERGY COST COMPARISON BETWEEN MBRAI AND PROPOSED CIM CORE

MBRAI [23]		Proposed	
Technology	45nm	Technology	45nm
Supply Voltage	1.1V	Supply Voltage	1V
System Clock	16.7MHz	System Clock	16.7MHz
Integral Amplifier	0.22mW	Regulator circuit	1.11uW
Core(256*256)	199.68mW	Core(256*256)	3.61mW

sequence is sent in from LSB to MSB and after 8 cycles of integration and charge redistribution, the output voltage V_{out} is 831.6mV. Then ADC converts it to digital result as 8'b10101011. The theoretical results of the output voltage and digital result are 831.5mV and 8'b10101011, respectively. Therefore, the design achieves its functional requirement.

2) *Resistance Measurement Verification*: Fig.7 presents the resistance measuring process of one 1R1T unit where the state of the switches in the same bit line is simulated. The output voltage is set to 1V at first and the integration phase is started at 190 ns. Since only one 1R1T is working, the integrating current is small and thus the integrating time is set to 110 ns which is much longer than that of MAC operation. After integration, the sampling phase (i.e. the charge redistribution phase) starts at 440ns and the output voltage is 0.994 V. Then the ADC converts it to digital output.

B. Performance Evaluation

1) *Circuit Level Performance*: Table I shows the dynamic performance comparison between MBRAI and the proposed core. The computing speed, SFDR, SNDR, ENOB of the proposed CIM core are 1.85M/s, 59.13dB, 46.13dB, and 7.37bit, which are close to the performance indicators of MBRAI. Table II gives the power cost comparison between the proposed scheme and MBRAI. MBRAI consumes 0.22 mW on amplifiers for stable read voltage while the proposed circuit only consumes 1.11uW on the regulator circuit, and the total power consumption of the core(256*256) is reduced by 98.2%.

2) *Core Level Comparison*: The core level comparison between the proposed scheme and the other CIM core schemes is shown in Table III. The simulation results show that the proposed design achieves energy efficiency as high as 553.01 TMACs/s/W in 2-bit input 2-bit weight pattern, 205.30 TMACs/s/W in 4-bit input 4-bit weight pattern, and 33.63 TMACs/s/W in 8-bit input 8-bit weight pattern. Compared with MBRAI, whose energy efficiency is 77.76 TMACs/s/W in 1-bit input 3-bit weight pattern, 38.8 TMACs/s/W in 2-

bit input 3-bit weight pattern, and 0.61 TMACs/s/W in 8-bit input 8-bit weight pattern, the proposed scheme achieves much higher energy efficiency (55.13 times in 8-bit input 8-bit weight pattern). Though [27] achieves a low average power consumption in fixed-4 input and fixed-4 weight pattern, the throughput of the core is limited by the rate coding scheme. Meanwhile, the power consumption in [27] will increase with the input value increase, which may achieve a much higher power consumption in practice. Comparing with other CIM schemes, the proposed CIM core achieves better energy efficiency.

3) *Network Level Comparison*: The accuracy and energy estimation comparison between the proposed scheme and other RRAM based schemes is shown in Table IV. Though the binary CIM scheme performs well on small-scale networks, the performance of this scheme on large-scale networks is much worse than the multibit based schemes because of its 1-bit quantization. When considering the energy cost, our scheme reduces 99.81% of inference energy per image compared with the binary CIM scheme and 98.17% compared with MBRAI for LeNet on MNIST. The proposed scheme also reduces 99.69% inference energy per image compared with the binary CIM scheme and 98.64% compared with MBRAI for AlexNet on ILSVRC 2012. Therefore, by abandoning the amplifiers, the proposed scheme achieves much lower inference energy cost.

C. Robustness Analysis

1) *Linearity Analysis*: The linearity comparison of integration results under different initial integrating voltage (0.7~1V) between the integrator without 1T1R unit position switching, integrator without T_0 , and integrator with T_0 is shown in Fig. 8(a), Fig. 8(b), and Fig. 8(c), respectively. The Differential Nonlinearity (DNL) and Integration Nonlinearity (INL) are used to evaluate the performance. The INL/DNL is (-1.66~0.89)/(-2.19~1.95) LSB for the integrator without 1T1R unit position switching, (-0.63~0.95)/(-1.24~1.35) LSB for integrator without T_0 , and (-0.40~0.60)/(-0.79~0.87) LSB for the integrator with T_0 which confirms that the linearity of the integration process is greatly improved by 1T1R unit position switching and T_0 . Fig. 9(a) and Fig. 9(b) present the linearity evaluation of the proposed integral multiplier with different input and weight by the code density measurement. The circuit achieves INL/DNL of (-0.51~0.36)/(-0.35~0.28) LSB, (-0.60~0.001)/(-0.14~0.17) LSB corresponding to input value and weight, respectively. The linearity comparison of the integral multiplier under different input lines between the circuit with regulator and without regulator is shown in Fig. 9(c) and Fig. 9(d), respectively. The INL/DNL is (-2.01~-0.38)/(0.01~0.01) LSB for the circuit with regulator and (-12.7~4.26)/(-0.2~0.62) for the circuit without regulator, which shows that the linearity in terms of the number of input lines is significantly improved by the regulator for providing a relatively stable drain voltage of 1R1T when the loads of bit line change.

2) *PVT Simulation*: To verify the robustness of the circuit, different combinations of process, voltage, and temperature

TABLE III
CORE LEVEL COMPARISON BETWEEN THE PROPOSED SCHEME AND OTHER CIM SCHEMES

Structure	Technology	Crossbar Size	Weight/Data Bit	Throughput(GMACS)	Power(mW)	Efficiency(TMAs/s/W)
SINWP [21] [22]	55nm	256*512	fixed-3/fixed-1	—	—	53.17
			fixed-3/fixed-2	—	—	21.9
MBRAI [23]	45nm	256*256	fixed-3/fixed-1	1524	19.6	77.76
			fixed-3/fixed-2	1040	26.8	38.8
			fixed-8/fixed-8	121.4	199.68	0.61
A 22nm 2Mb ReRAM CIM Macro [26]	22nm	512*512	fixed-2/fixed-1	—	—	121.38
			fixed-4/fixed-2	—	—	45.52
			fixed-4/fixed-4	—	—	28.93
Proposed	45nm	256*256	fixed-2/fixed-2	1092.2	1.975	553.01
			fixed-4/fixed-4	546.1	2.66	205.30
			fixed-8/fixed-8	121.4	3.61	33.63
A CIM SRAM Macro in 7nm FinFET CMOS [27]	7nm	4kb	fixed-4/fixed-4	186.2	1.06	175.5

TABLE IV
ACCURACY AND ENERGY ESTIMATION OF DIFFERENT RRAM-BASED SCHEME

Network	The Number of Operations	Structure	System Frequency	Data Bit	Crossbar Size	top-1 error Rate	Energy(uJ/img)	Saving(%)
LeNet on MNIST	0.42M	BNN+ADCs [25]	100MHz	1	128*128	1.40%	6.68	99.81%
		MBRAI [23]	25MHz	8	256*256	0.97%	0.71	98.17%
		Proposed	16.7MHz	8	256*256	0.90%	0.013	—
AlexNet on ILSVRC 2012	720M	BNN+ADCs [25]	100MHz	1	128*128	73.90%	5.42E+03	99.69%
		MBRAI [23]	25MHz	8	256*256	44.16%	1.23E+03	98.64%
		Proposed	16.7MHz	8	256*256	43.60%	16.65	—

TABLE V
PVT SIMULATION ON ENOB

Process	ff				ss				tt
Temperature(°C)	-40				80				27
Voltage(V)	0.9	1.1	0.9	1.1	0.9	1.1	0.9	1.1	1
ENOB(bit)	7.36	7.3	7.25	7.1	7.35	7.27	7.05	7.03	7.37

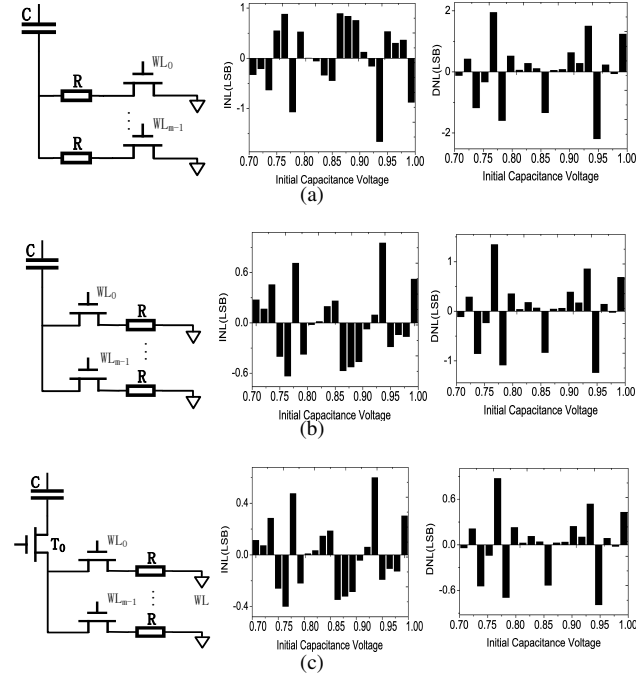


Fig. 8. The INL/DNL comparison of integration results under different integrating voltage(0.7~1V) between (a) integrator without 1T1R unit position switching, (b) integrator without T0, and (c) integrator with T0.

are chosen to do the PVT simulation where ENOB is used to evaluate the core's performance. The ENOBs in these PVT combinations are all greater than 7 bits as shown in Table

V which indicates that the proposed circuit is reliable with variations of process, voltage, and temperature.

3) *Quantization and Mapping Methods Comparison:* To add the impact of resistance distribution into the weight of the neural network, the resistance reading phase is needed when the ADC is used to read the resistance of the RRAM array. To make things easy, the process of ADC reading 1R1T circuit with fixed resistance is firstly simulated by 1400 Monte Carlo simulations to evaluate the impact of the transistor variation, then the resistance inconsistency is evaluated by adding a normalized Gaussian distribution. The normalized distribution of RRAM array read by ADC is shown in Fig.10, where the standard deviation of the normalized Gaussian distribution is 0.2. Fig. 11 shows the comparison of 1400 Monte Carlo simulations on the computation error of combination of input 180, weight 75, number of input lines 128 between normal mapping and bit line weight mapping method. The average value and the standard deviation of the error in normal mapping method are 0.124 LSB and 1.744LSB, respectively, while those of the errors in bit line weight mapping method are 0.013 LSB and 0.104 LSB, respectively. The mapping result indicates that the bit line weight mapping method significantly improves our CIM core's robustness to variations of device inconsistency.

To test the effect of the bit line weight mapping method on network level, three quantization and mapping methods are simulated. The first one is normal binary quantization and mapping method, which quantifies the weight to digital 8-bit value and set the resistance HRS/LRS according to the corresponding digital bit 0/1. The second one is resistance based quantization and mapping method that quantifies the weight according to Eq. 25. The third one is resistance based quantization and bit line weight mapping method proposed in this paper. Fig. 12(a) shows the quantization error ratio (sum of absolute values of quantization error/sum of absolute

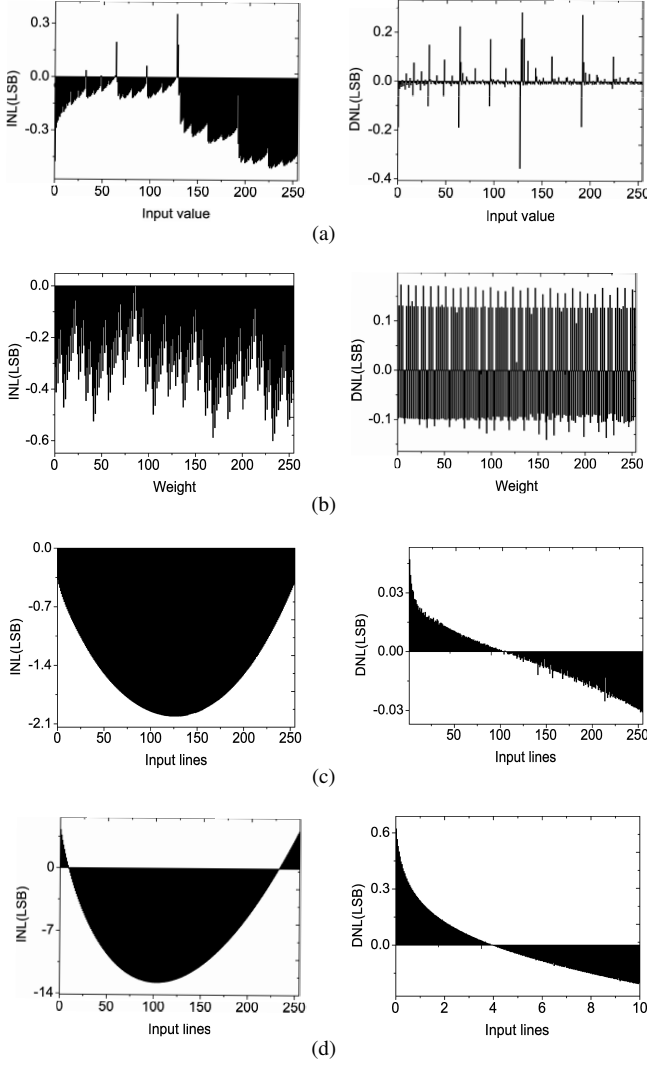


Fig. 9. The evaluation of linearity in terms of (a) different input(0-255) and (b) different weight(0-255) and the INL/DNL comparison between (c) integral multiplier with regulator and (d) integral multiplier without regulator under different input lines(1-256).

values of weight) and the loss of top-1 accuracy comparison between three methods under different quantization bits (the deviation of normalized resistance is 0.2) and different standard deviation of normalized resistance distribution (the quantization bits is 8) on AlexNet and ILSVRC 2012; Fig. 12(b) presents the quantization error ratio and the loss of top-1 accuracy comparison between quantization methods with different quantization bit (the deviation of normalized resistance is 0.2) and standard deviation of the resistance distribution (the quantization bits is 8) on VGG16 and ILSVRC 2012. As shown in Fig. 12, the optimized quantization and bit line weight mapping method helps reduce the quantization errors and improve the inference accuracy both on AlexNet and VGG16. For example, the accuracy loss in 8-bit mode with 0.2 deviation on AlexNet are 2.97% and 0.51% for normal binary mapping method and bit line weight mapping method, respectively, and those on VGG16 are 2.70% and 0.39% for normal binary mapping method and bit line weight mapping method, respectively. What's more, with the uncertainty of the

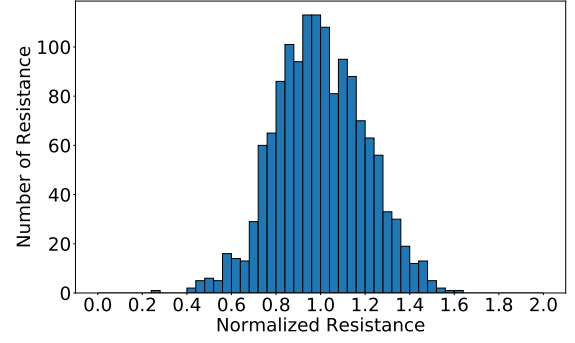


Fig. 10. Normalized resistance distribution read by ADC where the standard deviation of normalized Gaussian distribution is 0.2.

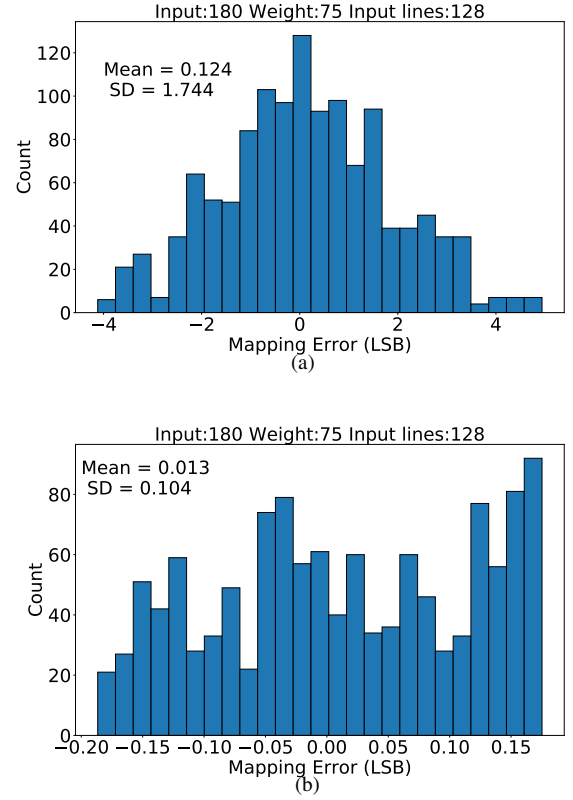


Fig. 11. Comparison of 1400 Monte Carlo simulations on the computation error of combination of input 180, weight 75, number of input lines 128 between (a) normal mapping and (b) bit line weight mapping method.

resistance increasing the effect of the optimization is more evident.

V. CONCLUSION

In this paper, an 8-bit RRAM based CIM core with regulated passive neuron and bit line weight mapping method has been proposed. The non-linearity brought by the passive integrator and the errors caused by quantization and the cell to cell variation have been discussed. To address the above issues, the detailed regulated integral multiplier and the bit line weight mapping method have been presented. The circuit level simulation has shown that the proposed CIM core achieves 3.61mW on power consumption with the size of 256*256

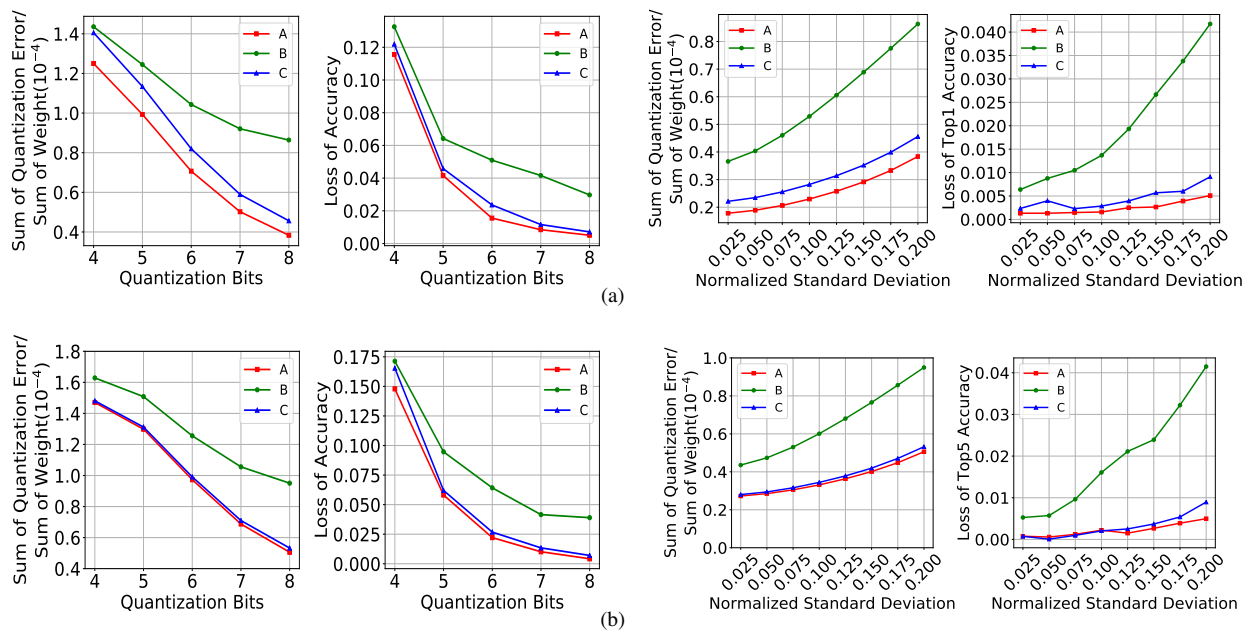


Fig. 12. The accuracy comparison between A: Resistance based quantization and bit line weight mapping method, B: Normal binary quantization and mapping method, and C: Resistance based quantization and normal mapping method. (a) The left two figures are quantization error ratio (sum of absolute values of quantization error/sum of absolute values of weight) and loss of top-1 accuracy of AlexNet on ILSVRC 2012 with different quantization bits (the deviation of normalized resistance is 0.2) while the right two are quantization error ratio and loss of top-1 accuracy of AlexNet on ILSVRC 2012 with different standard deviation of normalized resistance distribution (the quantization bits is 8). (b) The left two figures are quantization error ratio and loss of top-1 accuracy of VGG16 on ILSVRC 2012 with different quantization bits (the deviation of normalized resistance is 0.2) while the right two are quantization error ratio and loss of top-1 accuracy of VGG16 on ILSVRC 2012 with different standard deviation of normalized resistance distribution (the quantization bits is 8).

in 8-bit input and 8-bit weight mode, which is reduced by 98.2% compared with MBRAI while the SFDR and SNDR of the CIM core achieve 59.13 dB and 46.13 dB, respectively. The network level simulation has shown that the CIM core achieves 0.90% top-1 error rate with 0.013 uJ/img on LeNet and 43.60% top-1 error rate with 16.65 uJ/img on AlexNet, which are better than other schemes. The linearity and PVT simulation has been done to verify the robustness of the circuit. The simulation on mapping methods has shown that compared with normal mapping method, the proposed bit line weight mapping scheme achieves better performance which improves the top-1 accuracy by 2.46% and 3.47% for AlexNet and VGG16 on ILSVRC 2012 in 8-bit mode.

ACKNOWLEDGMENT

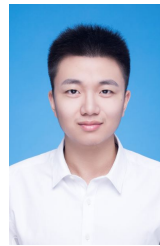
This work was supported by the Major Scientific Research Project of Zhejiang Lab (No. 2019KC0AD02).

REFERENCES

- [1] K. Chang and M. Chiang. Design of data reduction approach for aiot on embedded edge node. In *2019 IEEE 8th Global Conference on Consumer Electronics (GCCE)*, pages 899–900, 2019.
- [2] H. Pham, M. Nguyen, and C. Sun. Aiot solution survey and comparison in machine learning on low-cost microcontroller. In *2019 International Symposium on Intelligent Signal Processing and Communication Systems (ISPACS)*, pages 1–2, 2019.
- [3] G. W. Burr, R. M. Shelby, C. di Nolfo, J. W. Jang, R. S. Shenoy, P. Narayanan, K. Virwani, E. U. Giacometti, B. Kurdi, and H. Hwang. Experimental demonstration and tolerancing of a large-scale neural network (165,000 synapses), using phase-change memory as the synaptic weight element. In *2014 IEEE International Electron Devices Meeting*, pages 29.5.1–29.5.4, 2014.
- [4] K. Huang, Y. Ha, R. Zhao, A. Kumar, and Y. Lian. A low active leakage and high reliability phase change memory (pcm) based non-volatile fpga storage element. *IEEE Transactions on Circuits and Systems I: Regular Papers*, 61(9):2605–2613, 2014.
- [5] L. Zhang, W. Kang, H. Cai, P. Ouyang, L. Torres, Y. Zhang, A. Todri-Sanial, and W. Zhao. A robust dual reference computing-in-memory implementation and design space exploration within stt-mram. In *2018 IEEE Computer Society Annual Symposium on VLSI (ISVLSI)*, pages 275–280, 2018.
- [6] S. Jain, A. Ranjan, K. Roy, and A. Raghunathan. Computing in memory with spin-transfer torque magnetic ram. *IEEE Transactions on Very Large Scale Integration (VLSI) Systems*, 26(3):470–483, 2018.
- [7] Y. Pan, P. Ouyang, Y. Zhao, W. Kang, S. Yin, Y. Zhang, W. Zhao, and S. Wei. A mlc stt-mram based computing in-memory architecture for binary neural network. In *2018 IEEE International Magnetism Conference (INTERMAG)*, pages 1–1, 2018.
- [8] S. Jain, A. Ranjan, K. Roy, and A. Raghunathan. Computing in memory with spin-transfer torque magnetic ram. *IEEE Transactions on Very Large Scale Integration (VLSI) Systems*, 26(3):470–483, 2018.
- [9] H. P. Wong, H. Lee, S. Yu, Y. Chen, Y. Wu, P. Chen, B. Lee, F. T. Chen, and M. Tsai. Metaloxide rram. *Proceedings of the IEEE*, 100(6):1951–1970, 2012.
- [10] W. Wan, R. Kubendran, S. B. Eryilmaz, W. Zhang, Y. Liao, D. Wu, S. Deiss, B. Gao, P. Raina, S. Joshi, H. Wu, G. Cauwenberghs, and H. P. Wong. 33.1 a 74 tmacs/w cmos-rram neurosynaptic core with dynamically reconfigurable dataflow and in-situ transposable weights for probabilistic graphical models. In *2020 IEEE International Solid-State Circuits Conference - (ISSCC)*, pages 498–500, 2020.
- [11] Z. Yang and L. Wei. Logic circuit and memory design for in-memory computing applications using bipolar rams. In *2019 IEEE International Symposium on Circuits and Systems (ISCAS)*, pages 1–5, 2019.
- [12] Z. Liu, E. Ren, F. Qiao, Q. Wei, X. Liu, L. Luo, H. Zhao, and H. Yang. Ns-cim: A current-mode computation-in-memory architecture enabling near-sensor processing for intelligent iot vision nodes. *IEEE Transactions on Circuits and Systems I: Regular Papers*, pages 1–14, 2020.
- [13] C. Xue and M. Chang. Challenges in circuit designs of nonvolatile-memory based computing-in-memory for ai edge devices. In *2019 International SoC Design Conference (ISOCC)*, pages 164–165, 2019.
- [14] W. Chen, W. Khwa, J. Li, W. Lin, H. Lin, Y. Liu, Y. Wang, Huaqiang

Wu, Huazhong Yang, and M. Chang. Circuit design for beyond von neumann applications using emerging memory: From nonvolatile logics to neuromorphic computing. In *2017 18th International Symposium on Quality Electronic Design (ISQED)*, pages 23–28, 2017.

- [15] G. W. Burr, P. Narayanan, R. M. Shelby, S. Sidler, I. Boybat, C. di Nolfo, and Y. Leblebici. Large-scale neural networks implemented with non-volatile memory as the synaptic weight element: Comparative performance analysis (accuracy, speed, and power). In *2015 IEEE International Electron Devices Meeting (IEDM)*, pages 4.4.1–4.4.4, 2015.
- [16] J. Jang, S. Park, G. W. Burr, H. Hwang, and Y. Jeong. Optimization of conductance change in prlxcmno₃-based synaptic devices for neuromorphic systems. *IEEE Electron Device Letters*, 36(5):457–459, 2015.
- [17] A. Fumarola, P. Narayanan, L. L. Sanches, S. Sidler, J. Jang, K. Moon, R. M. Shelby, H. Hwang, and G. W. Burr. Accelerating machine learning with non-volatile memory: Exploring device and circuit tradeoffs. In *2016 IEEE International Conference on Rebooting Computing (ICRC)*, pages 1–8, 2016.
- [18] E. Giacomini, T. Greenberg-Toledo, S. Kvatinisky, and P. Gaillardon. A robust digital rram-based convolutional block for low-power image processing and learning applications. *IEEE Transactions on Circuits and Systems I: Regular Papers*, 66(2):643–654, 2019.
- [19] M. Hu, J. P. Strachan, Z. Li, E. M. Grafals, N. Davila, C. Graves, S. Lam, N. Ge, J. J. Yang, and R. S. Williams. Dot-product engine for neuromorphic computing: Programming 1t1m crossbar to accelerate matrix-vector multiplication. In *2016 53rd ACM/EDAC/IEEE Design Automation Conference (DAC)*, pages 1–6, 2016.
- [20] A. Shafiee, A. Nag, N. Muralimanohar, R. Balasubramanian, J. P. Strachan, M. Hu, R. S. Williams, and V. Srikumar. Isaac: A convolutional neural network accelerator with in-situ analog arithmetic in crossbars. In *2016 ACM/IEEE 43rd Annual International Symposium on Computer Architecture (ISCA)*, pages 14–26, 2016.
- [21] C. Xue, W. Chen, J. Liu, J. Li, W. Lin, W. Lin, J. Wang, W. Wei, T. Chang, T. Chang, T. Huang, H. Kao, S. Wei, Y. Chiu, C. Lee, C. Lo, Y. King, C. Lin, R. Liu, C. Hsieh, K. Tang, and M. Chang. 24.1 a 1mb multibit rram computing-in-memory macro with 14.6ns parallel mac computing time for cnn based ai edge processors. In *2019 IEEE International Solid-State Circuits Conference - (ISSCC)*, pages 388–390, 2019.
- [22] C. Xue, W. Chen, J. Liu, J. Li, W. Lin, W. Lin, J. Wang, W. Wei, T. Huang, T. Chang, T. Chang, H. Kao, Y. Chiu, C. Lee, Y. King, C. Lin, R. Liu, C. Hsieh, K. Tang, and M. Chang. Embedded 1-mb rram-based computing-in-memory macro with multibit input and weight for cnn-based ai edge processors. *IEEE Journal of Solid-State Circuits*, 55(1):203–215, 2020.
- [23] S. Zhang, K. Huang, and H. Shen. A robust 8-bit non-volatile computing-in-memory core for low-power parallel mac operations. *IEEE Transactions on Circuits and Systems I: Regular Papers*, 67(6):1867–1880, 2020.
- [24] A. Biswas and A. P. Chandrakasan. Conv-ram: An energy-efficient sram with embedded convolution computation for low-power cnn-based machine learning applications. In *2018 IEEE International Solid-State Circuits Conference - (ISSCC)*, pages 488–490, 2018.
- [25] T. Tang, L. Xia, B. Li, Y. Wang, and H. Yang. Binary convolutional neural network on rram. In *2017 22nd Asia and South Pacific Design Automation Conference (ASP-DAC)*, pages 782–787, 2017.
- [26] C. Xue, T. Huang, J. Liu, T. Chang, H. Kao, J. Wang, T. Liu, S. Wei, S. Huang, W. Wei, Y. Chen, T. Hsu, Y. Chen, Y. Lo, T. Wen, C. Lo, R. Liu, C. Hsieh, K. Tang, and M. Chang. 15.4 a 22nm 2mb rram compute-in-memory macro with 121-28tops/w for multibit mac computing for tiny ai edge devices. In *2020 IEEE International Solid-State Circuits Conference - (ISSCC)*, pages 244–246, 2020.
- [27] Q. Dong, M. E. Sinangil, B. Erbagci, D. Sun, W. Khwa, H. Liao, Y. Wang, and J. Chang. 15.3 a 351tops/w and 372.4gops compute-in-memory sram macro in 7nm finfet cmos for machine-learning applications. In *2020 IEEE International Solid-State Circuits Conference - (ISSCC)*, pages 242–244, 2020.



Yewei Zhang (Student Member, IEEE) received the bachelors degree from College of Information Science & Electronic Engineering, Zhe Jiang University in 2018. He is currently studying for a master's degree at College of Information Science & Electronic Engineering, Zhe Jiang University. He is interested in in-memory computing and non-volatile memories.



Kejie Huang (Senior Member, IEEE) received the Ph.D. degree from the Department of Electrical Engineering, National University of Singapore (NUS), Singapore, in 2014. He has been a Principal Investigator with the College of Information Science Electronic Engineering, Zhejiang University (ZJU), since 2016. Prior to joining ZJU, he has spent five years at the IC design industry, including Samsung and Xilinx, two years in the Data Storage Institute, Agency for Science Technology and Research (A*STAR), and another three years in the Singapore University of Technology and Design (SUTD), Singapore. He has authored or coauthored more than 30 scientific articles in international peer-reviewed journals and conference proceedings. He holds four granted international patents, and another eight pending ones. His research interests include low power circuits and systems design using emerging non-volatile memories, architecture and circuit optimization for reconfigurable computing systems and neuromorphic systems, machine learning, and deep learning chip design. He currently serves as the Associate Editor of the IEEE TRANSACTIONS ON CIRCUITS AND SYSTEMS-PART II: EXPRESS BRIEFS.



RuiXiao (Student Member, IEEE) received her bachelors degree from the School of Information Science and Electronic Engineering, Zhejiang University in 2019. She is currently working for her Ph.D. degree in the School of Information Science and Electronic Engineering, Zhejiang University. Her research interests include in-memory computing, non-volatile memories, and neuromorphic systems.



Haibin Shen is currently a Professor with Zhejiang University, a member of the second level of 151 talents project of Zhejiang Province, and a member of the Key Team of Zhejiang Science and Technology Innovation. His research interests include learning algorithm, processor architecture, and modeling. His research achievement has been used by many authority organizations. He has published more than 100 papers on academic journals, and he has been granted more than 30 patents of invention. He was a recipient of the First Prize of Electronic Information Science and Technology Award from the Chinese Institute of Electronics, and has won a second prize at the provincial level.